

First-principles high-throughput screening of bulk piezo-photocatalytic materials for sunlight-driven hydrogen production

Zhao Liu,^{1,2} Biao Wang,^{1,2} Dewei Chu,³ and Claudio Cazorla⁴

¹*School of Materials Science and Engineering, Dongguan University of Technology, Dongguan 523808, China*

²*Research Institute of Interdisciplinary Science, Dongguan University of Technology, Dongguan 523808, China*

³*School of Materials Science and Engineering, UNSW Sydney, Sydney, NSW 2052, Australia*

⁴*Departament de Física, Universitat Politècnica de Catalunya, Campus Nord B4-B5, Barcelona E-08034, Spain*

Finding cost-effective and efficient photocatalytic materials able to catalyse the water splitting reaction under visible light is one of the greatest challenges in current environmental material science. Despite that many photocatalysts are already known in the context of green hydrogen production, strategies to systematically and rationally modify their optoelectronic properties to achieve desired photocatalytic performance are yet to be established. Piezoelectric materials react to mechanical stimuli by adjusting their band gaps and band alignments, thus offering a possible route to precise photocatalyst design. However, piezo-photocatalysts are relatively scarce and have been seldom investigated to date. Here, we present a high-throughput screening of piezo-photocatalytic materials performed over $\sim 1,000$ bulk piezoelectrics that relies on a simple electrostatic model and first-principles calculations. A total of ~ 10 previously overlooked binary and tertiary bulk compounds are theoretically identified as highly promising piezo-photocatalysts due to their appropriate optoelectronic properties and superb band alignment tunability driven by uniaxial strain.

About three quarters of the hydrogen consumed annually worldwide, currently around 70 million tonnes, are produced by methane reforming, which generates about 830 million tons of CO₂ emissions [1, 2]. Aimed at curbing carbon emissions and motivated by the increasingly reduced costs of renewable electricity, there is growing interest in producing hydrogen from water electrolysis. However, generating the global hydrogen demand entirely from electricity would require an electricity consumption of 3600 TWh, which is not efficient from an energy resources point of view (e.g., it surpasses the annual electricity production of the European Union). Finding alternative means to produce clean hydrogen is therefore critical for attaining sustainable energy and industry futures. In this context, photocatalytic hydrogen production via solar water splitting emerges as one of the most promising solutions.

Splitting water molecules into oxygen and hydrogen under visible light is possible with the assistance of photocatalytic materials [3, 4]. Efficient photocatalytic materials should fulfill a number of stringent physical conditions like (Fig.1a–b): (1) the energy band gap, E_g ,

should be larger than 1.23 eV but smaller than ≈ 3.0 eV in order to be able to absorb the visible radiation from sunlight, (2) the bottom (top) of the conduction (valence) band, CBB (VBT), should be higher (lower) than the reduction (oxidation) potential H^+/H_2 (H_2O/O_2), HER (OER), which lies at -4.44 (-5.67) eV with respect to the vacuum level, and (3) the recombination rate of light-induced electron-hole charge carriers should be low. In addition to the above requirements, potential candidates should be also abundant and easy to synthesize. Therefore, finding suitable photocatalytic materials remains a challenging task.

Several chemical and nanostructuring approaches have been successful at improving the photocatalytic activity of archetypal inorganic compounds like TiO₂ and CeO₂ under sunlight [5–8]. However, the usual intricacy of nanostructuring methods along with the tremendous variability of the as-synthesized nanomaterials makes it difficult to identify general approaches for consistently enhancing the photocatalytic performance of crystals [9]. Consequently, progress in photocatalysis, and in particular in photocatalytic production of hydrogen, aided by rational design of materials remains limited [10].

Recently, some of us have shown by means of first-principles calculations that mechanical strains (biaxial and uniaxial) can modify the band-gap properties of transition-metal oxides in a significant and consistent manner [11, 12]. In practice, biaxial strains of 1–5% can be introduced in crystals by growing thin films on top of substrates that present a lattice mismatch [13, 14]. Similarly, uniaxial strains of comparable sizes can be realized in microstructured materials via mechanical actuation [15, 16] and/or exposure to ultrasound waves [17, 18]. Therefore, in view of the condition (1) above, mechanical stress in principle could be exploited to improve the photocatalytic activity of non-ideal materials by finely tuning their optoelectronic properties. However, achieving an adequate degree of predictability in the band-alignment variations of traditional semiconductors as induced by strain [see the condition (2) above] appears to be extremely challenging [11]. Such a lack of accomplishment critically hinders rational design of photocatalysts based on strain engineering.

Notwithstanding such limitations, a particular class of materials called piezoelectrics exhibit quantifiable and systematic band structure variations driven by mechanical stress. In response to a strain deformation, a finite electric field develops in the interior of piezoelectrics that

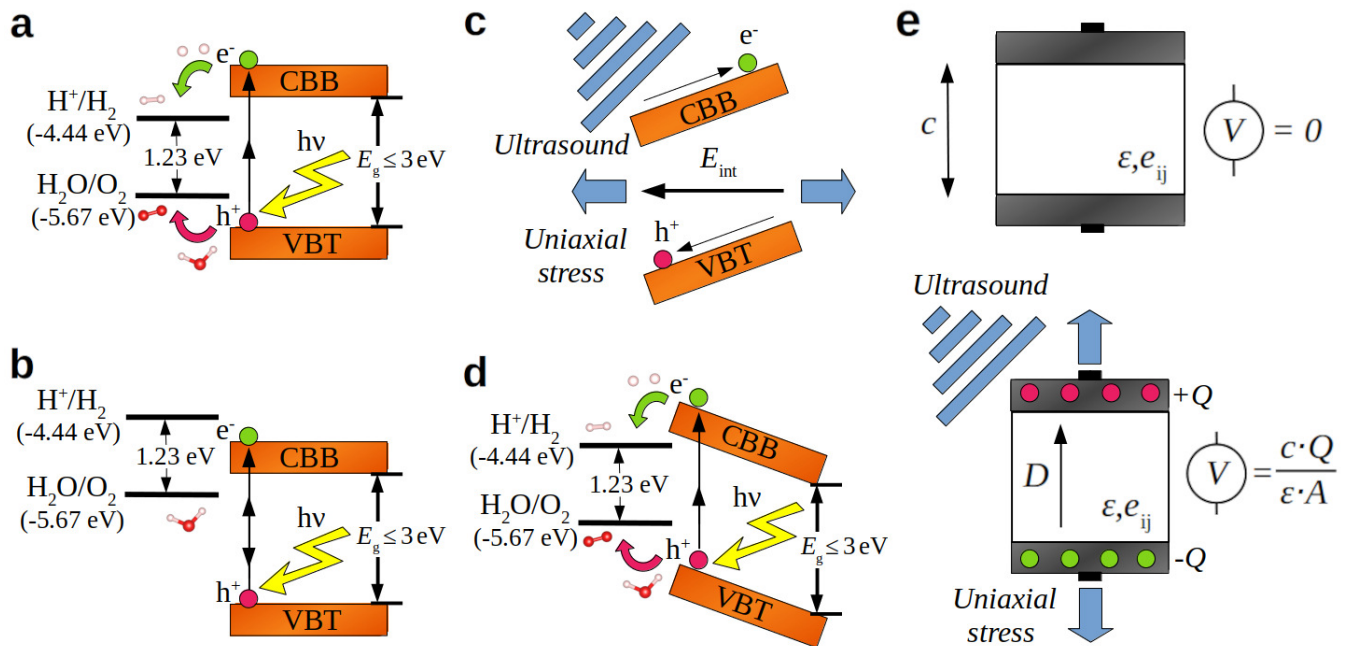


FIG. 1. Fundamental aspects of photocatalytic, piezoelectric and piezo-photocatalytic materials. **a** Opto-electronic properties of an ideal water-splitting photocatalyst; the conduction band bottom (CBB) and valence band top (VBT) of the photocatalyst perfectly straddle the OER and HER potentials as referred to the vacuum level. **b** Opto-electronic properties of a non-ideal water-splitting photocatalyst; the CBB and VBT of the photocatalyst fail to straddle the OER and HER potentials. **c** Application of uniaxial stress or ultrasound waves on a piezoelectric material induces an internal electric field and thus the appearance of a potential gradient. **d** Improvement of OER and HER straddling in a non-ideal photocatalyst that is piezoelectric achieved through uniaxial stress or ultrasound waves. **e** Simple parallel plate capacitor in which the dielectric material between the plates is a piezoelectric; upon application of uniaxial stress or ultrasound waves a finite voltage is created.

(i) introduces an approximately linear variation of the energy bands throughout the crystal, and (ii) reduces the recombination rate of migrating electron-hole pairs [see Fig.1c and conditions (2) and (3) above]. Moreover, piezoelectrics are non-centrosymmetric materials that encompass all pyroelectrics and ferroelectrics, hence they are abundant. These qualities are all very desirable for the rational engineering of novel materials with improved optoelectronic and photocatalytic properties (Fig.1d) [19] and some recent research have indeed focused on the study of archetypal “piezo-photocatalysts” like ZnO and BaTiO₃ [20–22]. Yet, a quantitative characterization and understanding of piezo-photocatalytic materials is lacking and the number of piezo-photocatalysts known to date is very limited.

In this work, we present a comprehensive first-principles computational study based on density functional theory (DFT) calculations that provides (i) a simple but physically insightful description of piezo-photocatalytic materials in terms of a piezoelectric plate capacitor (PPC) model, and (ii) a high-throughput screening of piezo-photocatalytic materials performed over a large database of $\sim 1,000$ bulk piezoelectrics [23] that relies on an easy-to-compute DFT descriptor. (Two-dimensional materials – e.g., g-C₃N₄ and GeS – and solid solutions – e.g., A_xA_{1-x}B_yB_{1-y}O₃ – are not included in

the inspected database [23] hence despite of their photocatalytic promise such families of compounds have been disregarded in the present study.) Based on our first-principles computational sieve, a number of previously overlooked binary and tertiary bulk compounds are identified as promising piezo-photocatalysts among which nitride (LaN and GaN), halide (PtF₄ and AgI), chalcogenide (BiTeCl, BiTeI, MgTe, CdS and ScCuS₂) and other inorganic (SiC) materials stand out due to their outstanding band-alignment tunability driven by uniaxial strain. Therefore, the present computational study has the potential to stimulate experimental synthesis of new piezo-photocatalytic materials able to boost the sustainable production of hydrogen based on solar water splitting.

RESULTS

In this section, a simple electrostatic model describing the band alignment rearrangements in a piezo-photocatalyst caused by uniaxial strain is first introduced along with an easy-to-compute first-principles descriptor of the resulting piezo-photocatalytic performance. Next, we present the main results of our high-throughput screening of piezo-photocatalytic ma-

materials performed over a large dataset of $\sim 1,000$ bulk piezoelectrics [23] followed by a careful quality check of the employed first-principles data. Finally, the outcomes of our refined high-throughput screening are confronted with explicit calculations of the piezo-photocatalytic performance of one of the most promising identified compounds when subjected to broad uniaxial strain conditions. For the sake of focus, and due to obvious limitations, other relevant aspects to photocatalytic activity different from band gap and band alignment features (e.g., surface molecular reactions and light absorption processes) mostly are left for future work.

Piezo-photocatalysts bulk modelling: The piezoelectric plate capacitor (PPC). To approximately model the band-alignment behavior of piezo-photocatalytic materials under stress, we start by examining the simple case of a parallel plate capacitor in which the dielectric material between the plates is piezoelectric (Fig.1e). Under open-circuit conditions and in the absence of mechanical stresses, the voltage drop among the plates of the capacitor, V , is null (we assume the spontaneous polarisation of the dielectric material to be zero). However, when a mechanical stress is applied on the capacitor V will be different from zero as a result of the accumulation of polarisation charges of different signs in the two capacitor plates. For the sake of simplicity, let us assume that (i) the mechanical stress (σ) is uniaxial and applied along the capacitor stacking direction, and (ii) the dielectric piezoelectric material is isotropic (Fig.1e). In such a case, the value of the potential drop can be evaluated as:

$$V = \frac{c \cdot Q}{\epsilon \cdot A} = \frac{c}{\epsilon} D, \quad (1)$$

where c represents the thickness of the capacitor, ϵ the dielectric constant of the piezoelectric material and D the charge per unit area accumulated in the plates. The value of the surface charge density can be determined via the isothermal piezoelectric stress constant of the dielectric material defined as:

$$e_{33} = \frac{\partial D}{\partial \eta}, \quad (2)$$

where $\eta \equiv \Delta c/c$ represents the stress-induced strain. Under small deformations it can be reasonably assumed that $D \approx e_{33}\eta$, hence the internal electric field that appears within the piezoelectric, E_{int} , can be also expressed in the linear approximation as:

$$E_{\text{int}}(\eta) = \frac{1}{c} V(\eta) = \frac{1}{c} \cdot \frac{\partial V}{\partial \eta} \eta \approx \frac{e_{33}}{\epsilon} \eta. \quad (3)$$

The following piezoelectric voltage coefficient can be defined from the formula above:

$$\alpha_{\eta} \equiv \frac{\partial V}{\partial \eta} = \frac{c}{\epsilon} e_{33}, \quad (4)$$

which describes the internal electrostatic potential variation induced by uniaxial strain. Based on the simple piezoelectric plate capacitor (PPC) model introduced here, it can be reasonably argued that to a first approximation the maximum band-alignment change induced by uniaxial strain on a piezoelectric thin film is:

$$\Delta V_i(\eta) \equiv V_i(\eta) - V_i(0) = -c E_{\text{int}}(\eta) = -\alpha_{\eta} \eta, \quad (5)$$

where i stands for either the conduction band bottom (CBB) or valence band top (VBT) energy levels. (Here, surface dipoles are assumed to not vary by effect of small η 's.)

From Eq.(5), it is readily shown that piezoelectric materials presenting large (small) α_{η} coefficients [Eq.(4)] will offer great (poor) band-alignment tunability as driven by uniaxial strain. Consequently, piezoelectric materials possessing energy band gaps in the range of $1.23 \lesssim E_g \lesssim 3.0$ eV (to absorb the sunlight visible radiation), small dielectric constants and large piezoelectric stress coefficients (the last two conditions as for maximizing ΔV_i), *a priori* should be regarded as promising piezo-photocatalysts. Moreover, large α_{η} coefficients imply large strain-induced internal electric fields [see Eqs.(3)–(4)] which are desirable for depleting the recombination rate of light-induced excitons (Fig.1c). It is noted that large piezoelectric stress constants typically are accompanied by also large dielectric constants [24, 25], thus it is naturally difficult to find materials with large band-alignment piezo tunability (i.e., large α_{η} values). This small set of conditions are not only physically insightful but also computationally convenient: the relevant quantities E_g , ϵ and e_{33} can be efficiently estimated via bulk first-principles DFT calculations [26–28]. As we will show in the next section, this circumstance can be exploited to conduct high-throughput computational searches of piezo-photocatalysts within large databases of piezoelectric materials that are publicly available [23].

It is important to note that the simple PPC model introduced here in principle should not be regarded as quantitatively accurate due to the involved simplifications (e.g., strain-induced E_g variations and surface dipole and surface relaxation effects have been neglected, and the assumed isotropic piezoelectric behaviour should not always be valid). Thus, any candidate piezo-photocatalyst identified on basis to the α_{η} descriptor should necessarily be put to test. In the next sections, we will comment on the extent of the possible limitations of the PPC model introduced in this section.

High-throughput piezo-photocatalysts screening. We performed a high-throughput computational search of piezo-photocatalysts over the Materials Project (MP) database containing about 1,000 different bulk piezoelectric compounds [23] (Methods). Figure 2 shows the steps followed in our high-throughput materials screening (Fig.2a) and the main results obtained from it (Fig.2b). Based on the PPC model introduced in the previous section and the DFT data available in the MP

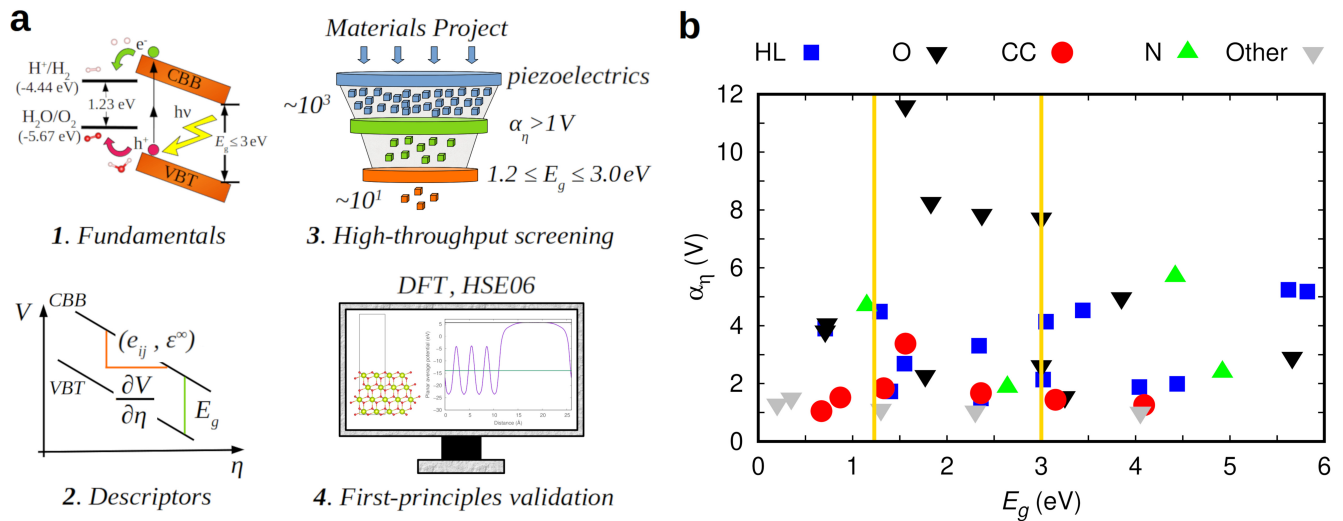


FIG. 2. High-throughput screening of piezo-photocatalytic materials for water splitting under visible light: strategy and results. **a** The adopted high-throughput screening strategy consists of a sequence of four steps. First, to understand the fundamentals of piezo-photocatalysts; second, to define a suitable set of easy-to-compute descriptors for piezo-photocatalytic materials; third, based on threshold descriptor values, to identify potential piezo-photocatalytic materials from the “Materials Project” database [23]; and fourth, to validate the results of the high-throughput screening by explicitly computing with first-principles methods the optoelectronic and band alignment properties of some of the identified piezo-photocatalysts. **b** High-throughput screening results. A total of 21 compounds were identified as potential piezo-photocatalytic materials for water splitting under visible light (Table I). The descriptor threshold values of $1.23 \lesssim E_g \lesssim 3.0$ eV are represented with gold vertical lines in the figure and only materials displaying $\alpha_\eta > 1$ V are considered. “HL” stands for materials mostly containing halide atoms (F, Cl, Br, I), “O” oxygen atoms, “CC” chalcogenide atoms (S, Se, Te), “N” nitrogen atoms, and “Other” refers to inorganic compounds not classified in the previous categories.

database, we applied two consecutive descriptor sieves on the reported bulk piezoelectrics. Compounds exhibiting a α_η coefficient larger than 1 V [Eq.(4)] were first selected (which amounted to 42, see Supplementary Table I; thus this condition encompasses the top $\approx 5\%$ of all the investigated materials in terms of band alignment tunability) and from them those fulfilling the band-gap condition $1.23 \lesssim E_g \lesssim 3.0$ eV were finally retrieved. A total of 21 compounds out of the initial $\sim 1,000$ piezoelectrics were tentatively identified as promising piezo-photocatalysts (Fig.2b), all of which are listed in Table I along with their most relevant properties.

Among the most promising piezo-photocatalysts we found oxide (e.g., KNbO_3 , BaTiO_3 , NaNbO_3 and KIO_3), nitride (e.g., LaN and $\text{Ge}_2\text{N}_2\text{O}$) and halide (e.g., PtF_4 , BaI_2 , BrF_3 and SeBr) materials, most of which have not been previously investigated in the context of green hydrogen production. In terms of band-alignment tunability, non-centrosymmetric oxide perovskites (i.e., KNbO_3 , BaTiO_3 and NaNbO_3) emerge as the clear winners since they exhibit huge α_η values larger than or close to 10 V. Several chalcogenides (e.g., BiTeCl and MgTe) and generic inorganic compounds (GaP and SiC) were also identified as potential photocatalysts, some of which appear to be especially promising in terms of reduced production costs (i.e., SiC).

It is worth noting that our first-principles based high-throughput search identified already well known piezo-

photocatalysts like BaTiO_3 [20–22] and KNbO_3 [29, 30]. Other piezoelectric materials frequently employed in optoelectronic applications like ZnO and InN [31] were not retrieved by our computational analysis because the corresponding E_g values appearing in the MP database were noticeably smaller than 1.23 eV. For example, for hexagonal ZnO (space group $P6_3mc$ and MP identity number mp – 2133) we estimated a large α_η coefficient value of 4.07 V, which turns out to be competitive with those of the top piezo-photocatalyst candidates listed in Table I; however, the ZnO band gap reported in the MP database amounts to 0.73 eV, which in principle would fail to properly straddle the OER and HER potentials [11].

Nonetheless, it is worth recalling here the inherent limitations of standard DFT approaches in estimating accurate band gaps in semiconductors due to the ubiquitous electronic self-interaction errors and other fundamental problems [32]. In particular, it is well known that common exchange-correlation functionals like LDA and GGA, which are computationally very affordable, tend to significantly underestimate E_g [34], and unfortunately (although also understandably) most of the results reported in the MP database are obtained with such standard DFT functionals. Thus, it is very likely that some of the candidate piezo-photocatalysts identified by our high-throughput search actually do not fulfill the band gap condition $E_g \lesssim 3.0$ eV. Similarly, it is also quite likely that some potentially good

piezo-photocatalysts have escaped our computational sieve due to the systematic DFT underestimation of their band gap (e.g., hexagonal ZnO [11], see next section). Furthermore, the reliability of the simple PPC model introduced in this work, upon which the present computational search has been built, needs to be assessed. Consequently, we undertook a careful evaluation of the MP data and PPC model employed in our computational search by performing supplementary first-principles calculations.

First-principles data refinement. We re-evaluated the structural, dielectric, piezoelectric and band gap properties of the 21 compounds listed in Table I by using stringent convergence parameters and fairly accurate DFT functionals (Methods). Specifically, we re-optimized the relevant atomic geometries with a large energy cut-off of 800 eV and a \mathbf{k} -point grid of spacing $2\pi \times 0.01 \text{ \AA}^{-1}$ for sampling of the first-Brillouin zone, using the PBEsol exchange-correlation functional [33] (this DFT functional has been consistently ranked among the best performers in terms of lattice parameters prediction for semiconductors [35]). The dielectric, piezoelectric and band gap properties of the PBEsol-relaxed structures were subsequently estimated with the range-separated hybrid HSE06 potential [34]. By proceeding in this manner, an homogeneous and consistently high level of numerical accuracy was guaranteed for all the investigated materials.

Figure 3a shows a comparison of the band gaps found in the MP database, E_g , and those estimated by following the strategy explained above, E_g^{HSE06} , for all the materials reported in Table I. As it was already expected, for most compounds E_g^{HSE06} turns out to be significantly larger than E_g (discrepancies amount to 60–110% in the worse cases; see deviations from the solid black line in Fig.3a). Upon correction of the usual band-gap underestimation obtained with local and semi-local DFT methods, 7 out of the 21 initially selected potential piezo-photocatalysts were discarded because their E_g^{HSE06} s were noticeably larger than 3 eV. The rejected materials were: NaNbO_3 , Na_2O_2 , BrF_3 , GeN_2O_2 , KNO_3 , BaI_2 and TlF (Fig.3a). It is noted that few compounds exhibiting energy band gaps marginally larger than 3 eV were not discarded (i.e., GaN , MgTe and SiC) since our estimations may still contain small numerical imprecisions of the order of 0.1 eV [32].

Likewise, Fig.3b shows a comparison of the piezoelectric voltage coefficients calculated with the DFT data found in the MP database, α_η , and the corresponding revised values estimated as explained above, α_η^{rev} , for all the compounds reported in Table I. In this occasion, the consensus between the two sets of equivalent data is somewhat improved as compared to the band-gap case, although from a quantitative point of view their agreement is still far from satisfactory (in few instances the discrepancies are larger than 100%; see deviations from the solid black line in Fig.3b). Interestingly, we appreci-

ate a quite systematic underestimation of α_η^{rev} obtained with local and semi-local DFT approaches, which for our present materials screening purposes does not represent a critical shortcoming (i.e., since we are interested in finding compounds with piezoelectric potential coefficients larger than a specific threshold value). Nevertheless, in the particular case of TlF and GaP we found that $\alpha_\eta^{\text{rev}} < 1 \text{ V}$ hence they were discarded as potential piezo-photocatalysts (it is worth noting that upon refinement of the MP data only TlF failed to fulfill the two conditions guiding our computational searches).

Given the typical E_g underestimation obtained with standard DFT approaches, in our data refinement we also considered those materials that, based on the available MP data, presented energy band gaps below 1.23 eV and fulfilled the condition $\alpha_\eta > 1 \text{ V}$ (Supplementary Table I). Consequently, a total of 9 additional compounds were picked up, among which only 3 passed our two-conditions sieve upon refinement of their data. Those three added potential piezo-photocatalysts are the oxide ZnO and the chalcogenides CdS and ScCuS_2 .

Therefore, as a result of our supplementary first-principles calculations, a total of 8 out of the 21 initially identified candidate materials were rejected while 3 out of the 21 initially rejected compounds were recovered, adding up to a total of 16 potentially good piezo-photocatalysts. This definitive set of promising compounds is listed in Table II along with their re-evaluated E_g^{HSE06} and α_η^{rev} values (additional materials properties can be found in the Supplementary Table II). There are appreciable quantitative differences among the two rankings of materials shown in Tables I and II that will be commented in the Discussion section. Next, we turn our attention to first-principles validation of the proposed PPC model and the computationally sieved piezo-photocatalytic materials.

First-principles validation of the PPC model and identified piezo-photocatalysts. For this crucial and computationally intensive part of our study, namely, explicit first-principles assessment of piezo-photocatalytic performances (i.e., not relying on materials descriptors) and testing of the PPC model, we selected SiC for several reasons. First, it is a very well-known and chemically simple material made of abundant and non-toxic elements that can be synthesised in a commercially large scale, hence from an applied point of view it is a very promising compound. Second, SiC exhibits several polymorphs some of which are piezoelectric (e.g., 2H and 4H) some of which are not (e.g., 3C), thus comparing their photocatalyst performances under uniaxial strain may be particularly meaningful. Third, despite of its high mechanical strength, several works in the literature have reported successful stabilisation of tensile uniaxial strains of $\approx 7 \%$ in nanostructured SiC [16], which is the maximum $|\eta|$ considered in the present work. Fourth, previous experimental works have already shown that unstrained SiC is a promising photo-

Formula	mp – ID	Space Group	c (Å)	ϵ (ϵ_0)	$ e_{33} $ ($C \cdot m^{-2}$)	E_g (eV)	α_η (V)	Type
KNbO ₃	4342	<i>P4mm</i> (99)	4.09	12.98	3.26	1.56	11.6	O
BaTiO ₃	5986	<i>P4mm</i> (99)	4.07	19.24	3.45	1.83	8.26	O
NaNbO ₃	4681	<i>Pmc2₁</i> (26)	6.39	29.60	3.22	2.37	7.85	O
KIO ₃	552729	<i>R3m</i> (160)	4.53	9.03	1.36	3.00	7.72	O
LaN	567290	<i>P6₃mc</i> (186)	4.74	20.48	1.79	1.15	4.69	N
PtF ₄	8943	<i>Fdd2</i> (43)	6.02	5.92	0.39	1.29	4.49	HL
BaI ₂	568536	<i>P6₃mc</i> (186)	7.94	14.52	0.67	3.05	4.14	HL
BiTeCl	28944	<i>P6₃mc</i> (186)	7.58	4.57	0.18	1.56	3.38	CC
BrF ₃	23297	<i>Cmc2₁</i> (36)	5.32	19.30	1.06	2.34	3.31	HL
SeBr	570589	<i>Aea2</i> (41)	8.02	4.72	0.14	1.55	2.69	HL
KNO ₃	6920	<i>R3m</i> (160)	4.44	4.22	0.22	3.00	2.62	O
Na ₂ O ₂	2340	<i>P6₃mc</i> (186)	5.69	5.36	0.19	1.77	2.28	O
TiF	558134	<i>Aem2</i> (39)	4.67	48.33	1.96	3.02	2.14	HL
Ge ₂ N ₂ O	4187	<i>Cmc2₁</i> (36)	5.42	8.18	0.25	2.64	1.87	N
BiTeI	22965	<i>P3m1</i> (156)	5.41	6.67	0.20	1.33	1.84	CC
GaN	804	<i>P6₃mc</i> (186)	3.89	11.65	0.46	1.74	1.75	N
AgI	22894	<i>P6₃mc</i> (186)	5.68	7.43	0.20	1.40	1.73	HL
MgTe	1039	<i>P6₃mc</i> (186)	5.58	8.31	0.22	2.36	1.67	CC
PI ₃	27529	<i>P6₃</i> (173)	7.79	2.96	0.05	2.36	1.49	HL
GaP	8882	<i>P6₃mc</i> (186)	4.72	13.02	0.27	1.30	1.11	Other
SiC	7140	<i>P6₃mc</i> (186)	3.75	11.32	0.28	2.30	1.05	Other

TABLE I. Materials classified as potentially good piezo-photocatalysts for water splitting under visible light according to our first-principles high-throughput screening. Compounds are ranked according to their α_η value estimated with the DFT data retrieved from the Materials Project (MP) database. “mp-ID” stands for the compound identification number in the MP database [23], “HL” for halide materials, “O” for oxides, “CC” for chalcogenides, “N” for nitrides, and “Other” for inorganic compounds not classified in the previous categories.

catalytic material for driving the water splitting reaction [36–39]. And fifth, SiC appears in the last position of the lists enclosed in Tables I and II hence positive evaluation of this compound in principle may also suggest suitable piezo-photocatalytic performances for the rest of materials ranked above it.

Figure 4a shows the impact of uniaxial strain on the band gap of SiC considering the piezoelectric polymorph 4H (hexagonal, space group *P6₃mc*). Strain-induced band lifting effects are fully taken into consideration in our first-principles DFT results. In the absence of any stress, the E_g^{HSE06} of 4H-SiC is indirect (Fig.4b) and approximately amounts to 3.3 eV. (It is noted that the SiC band gap reported in Table II corresponds to the 2H polymorph, which is slightly smaller; for our validation analysis we have selected 4H-SiC because this is one of the most well-known and easy to synthesise silicon carbide polymorphs.) Under either tensile or compressive uniaxial strains, E_g^{HSE06} is significantly reduced and its indirect nature is conserved (Fig.4b). The maximum η -induced band-gap reduction is achieved in the compressive side, where appropriate photocatalytic values below 3 eV are obtained for uniaxial strains larger than $\approx 3\%$ (in absolute value). Meanwhile, in the tensile side the strain-induced E_g^{HSE06} variation is less regular and suitable photocatalytic band-gap values are only attained at

uniaxial distortions larger than $\approx 5\%$. We have checked that the vibrational stability of the 4H-SiC polymorph is preserved upon application of the largest strains considered in this study (i.e., no imaginary lattice phonon bands appear in the two limit cases $\eta = \pm 7\%$, Fig.4c).

Figure 4d shows the variation of the 4H-SiC band alignments as induced by uniaxial strain (Methods). At zero strain, the VBT and CBB levels fail to correctly straddle the OER and HER potentials due to the existence of large negative offsets (e.g., the VBT level is approximately positioned 2 eV below the OER energy). When uniaxial strain is applied, however, the VBT and CBB levels are significantly displaced towards higher energies in the compressive side and towards lower energies in the tensile side. As a result, upon compressive uniaxial strains of $|\eta| > 4\%$ the band alignments of 4H-SiC are optimally positioned for straddling the OER and HER levels. It is also appreciated that the induced band-alignment changes can be regarded as roughly linear in η (at least locally). Therefore, based on our first-principles calculations, it is concluded that although unstrained 4H-SiC does not seem to be an optimal water-splitting photocatalyst its green hydrogen production performance can be substantially improved by means of compressive uniaxial strain (i.e., both the band gap and band alignments can be appropriately tuned for such an end). Analo-

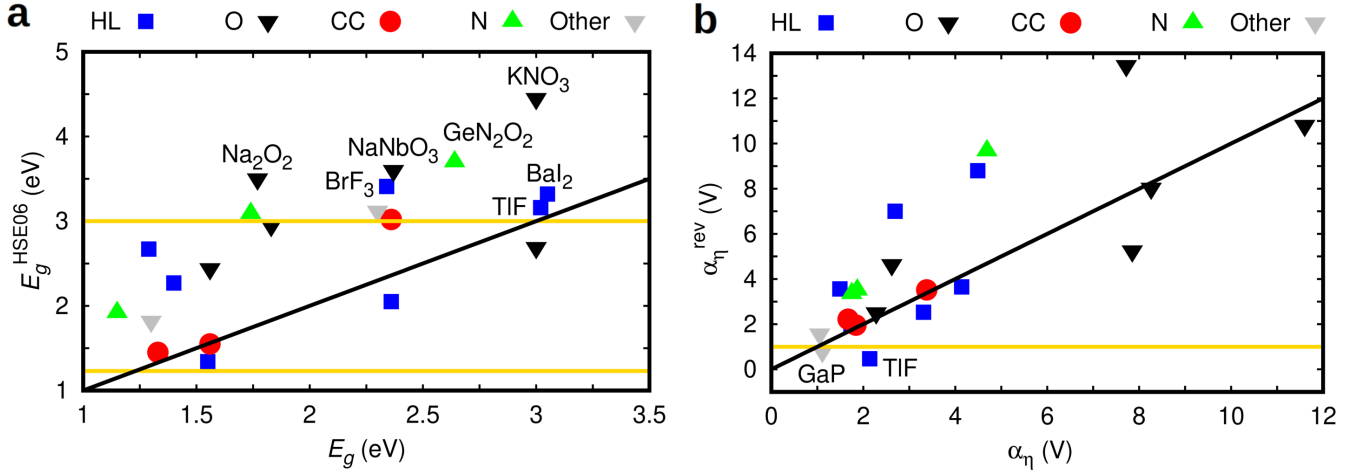


FIG. 3. Refinement of the first-principles data retrieved from the MP database. **a** MP band gap, E_g , versus HSE06 band gap, E_g^{HSE06} [34]. **b** Piezoelectric voltage coefficient calculated from the MP database, α_η , and from fully converged first-principles calculations based on the PBEsol [33] and HSE06 functionals, α_η^{rev} . As a result of our DFT data refinement, 8 out of the initially identified 21 potentially good piezo-photocatalysts for water splitting under visible light (Table I) were discarded (i.e., those named in the figures) since they did not fulfill either the condition of $1.23 \lesssim E_g^{\text{HSE06}} \lesssim 3.0$ eV and/or $\alpha_\eta^{\text{rev}} > 1$ V (gold lines). The solid black lines with a slope equal to one are guides to the eye for better appreciating the $E_g - E_g^{\text{HSE06}}$ and $\alpha_\eta - \alpha_\eta^{\text{rev}}$ discrepancies.

Formula	Space Group	E_g^{HSE06} (eV)	α_η^{rev} (V)	Drawbacks
KIO ₃	<i>R3m</i> (160)	2.69	13.46	Water soluble
KNbO ₃	<i>P4mm</i> (99)	2.44	10.81	–
LaN	<i>P6₃mc</i> (186)	1.92	9.67	–
PtF ₄	<i>Fdd2</i> (43)	2.67	8.80	High cost
BaTiO ₃	<i>P4mm</i> (99)	2.95	8.03	–
CdS	<i>P6₃mc</i> (186)	2.14	7.69	–
SeBr	<i>Aea2</i> (41)	1.34	7.00	Water soluble
ScCuS ₂	<i>P3m1</i> (156)	1.42	4.10	–
ZnO	<i>P6₃mc</i> (186)	2.73	4.07	–
PI ₃	<i>P6₃</i> (173)	2.05	3.56	Water reacting
BiTeCl	<i>P6₃mc</i> (186)	1.55	3.52	High cost
GaN	<i>P6₃mc</i> (186)	3.09	3.35	–
MgTe	<i>P6₃mc</i> (186)	3.02	2.22	High cost
AgI	<i>P6₃mc</i> (186)	2.27	1.99	–
BiTeI	<i>P3m1</i> (156)	1.45	1.96	High cost
2H – SiC	<i>P6₃mc</i> (186)	3.12	1.57	–

TABLE II. Revised list of potential piezo-photocatalysts for water splitting under visible light based on the refinement of the DFT data employed in our initial first-principles high-throughput screening. Compounds are ranked according to their revised piezoelectric voltage coefficient, α_η^{rev} . Potential practical drawbacks are indicated for each material.

gous band-alignment results are also obtained for the piezoelectric 2H-SiC polymorph (hexagonal, space group *P6₃mc*), although in this latter case straddling of the OER and HER levels is already attained in the absence

of structural distortions (Supplementary Fig.1).

The outcomes obtained for 4H-SiC are encouraging and qualitatively consistent with the simple PPC model introduced above, that is, in agreement with the potential energy variation predicted by Eq.(5). At the quantitative level, however, the accordance between the computed α_η coefficients and the explicitly estimated first-principles $dV/d\eta$ variations are fair but not exact. For instance, by taking numerical derivatives on the VBT data represented in Fig.4d we obtain a η -induced potential variation of 29 (6), 18 (6) and 16 (6) V for uniaxial strains of -7 , 0 and $+7\%$, respectively (numerical uncertainties are expressed within parentheses). Meanwhile, the physically equivalent α_η values calculated with Eq.(4) for the same lattice strains are 22, 1 and 23 V, respectively (i.e., the structural, dielectric and piezoelectric parameters defining the α_η coefficient have been recalculated at each uniaxial strain). Clearly, the numerical agreement between the two sets of α_η data is not satisfactory although in the two limit $|\eta|$ cases, for which the e_{33} coefficient largely increases (and so does α_η), the accordance is significantly improved. Several straightforward reasons explaining the lack of quantitative accuracy of the PPC model are: (i) the neglect of η -induced band gap variations (i.e., the VBT and CBB levels are treated identically whereas in practice they may react slightly different to strain, as it is shown in Fig.4d); (ii) the assumption of a perfectly isotropic piezoelectric medium (i.e., in practice, most piezoelectric tensors exhibit non-zero off-diagonal components hence the disregarded secondary lattice distortions may also accumulate charge along the principally strained direction and so influence the potential variation in the material); and (iii) the dis-

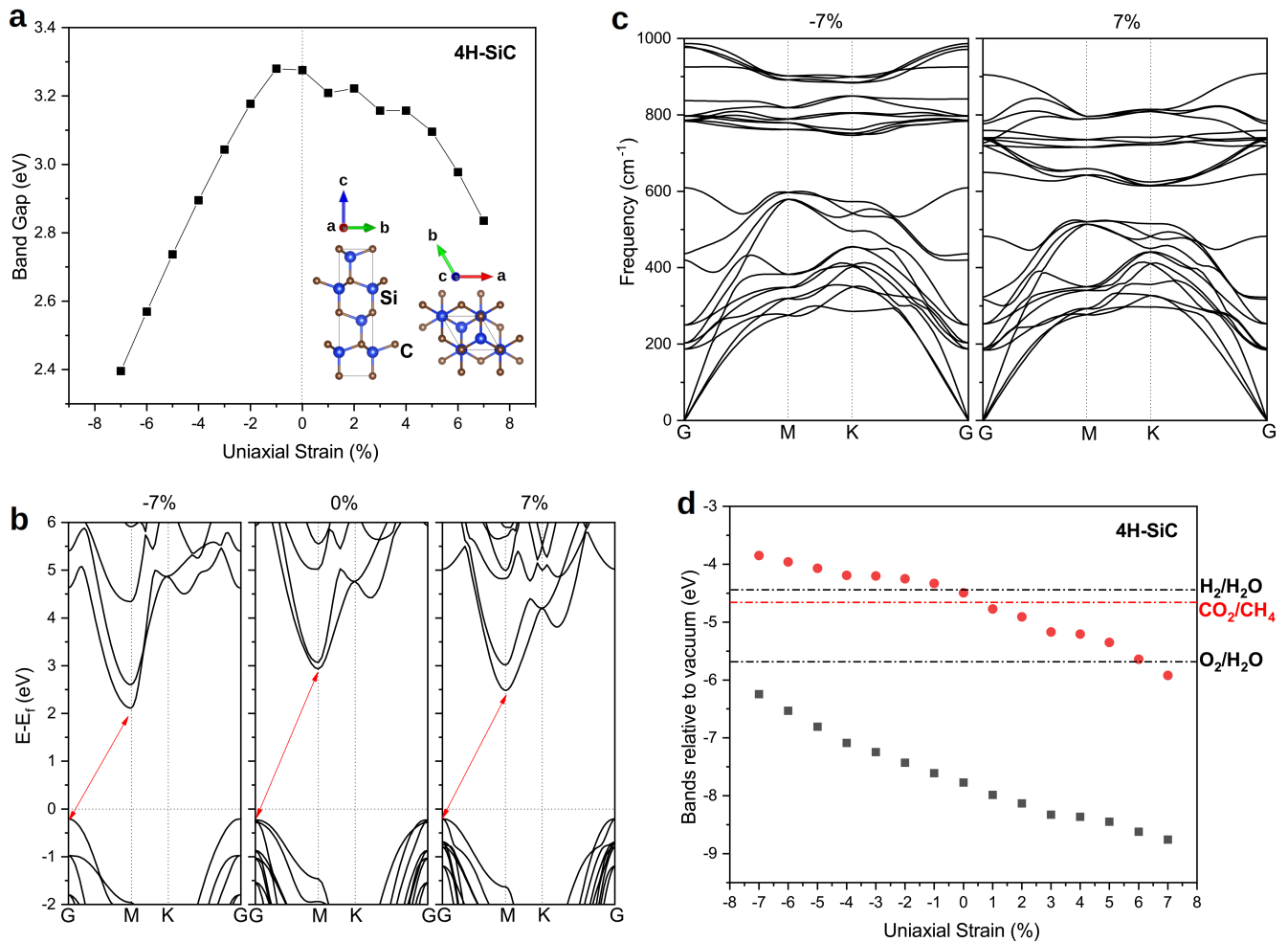


FIG. 4. First-principles analysis of the optoelectronic, vibrational, and band alignment properties of piezoelectric 4H-SiC. **a** Band-gap variation induced by uniaxial strain. **b** Dependence of the electronic band structure on uniaxial strain and reciprocal space point. **c** Phonon frequencies estimated as a function of uniaxial strain and reciprocal space point. **d** Effect of uniaxial strain on the band alignments of the crystal as referred to the vacuum level. The VBT and CBB energy levels are represented with solid grey squares and red circles, respectively.

regarding of surface dipole and surface relaxation effects.

It is worth commenting on the sign of the ΔV_i shift ($i = \text{VBT, CBB}$) as induced by η . In standard piezoelectrics, piezoelectric and piezoelectric voltage (Eq.4) coefficients are positively defined ($e_{33}, \alpha_\eta > 0$); thus, according to the PPC model, under tensile uniaxial strain ($\eta > 0$) the electrostatic potential in the interior of the material should rise as referred to the zero vacuum level (Eq.5 and Fig.1c). Conversely, under compressive uniaxial strain ($\eta < 0$) the electrostatic potential in the interior of the piezoelectric should come closer to the zero vacuum level (Eq.5). These ΔV_i trends predicted by the PPC model in fact are clearly reproduced by the DFT results enclosed in Fig.4d. Furthermore, we performed supplementary band alignment calculations for an anomalous piezoelectric material exhibiting negative piezoelectric and piezoelectric voltage coefficients ($e_{33}, \alpha_\eta < 0$). In this latter case, the expected η -induced ΔV_i shifts are opposite to

those just explained, namely, tensile (compressive) uniaxial strain reduces (increases) the electrostatic potential in the interior of the material as referred to the zero vacuum level. Consistently, our DFT calculations reproduce the potential trends anticipated by Eq.(5) also in this case (Supplementary Fig.2).

Figure 5 shows equivalent results to those just explained for 4H-SiC but obtained for the non-piezoelectric polymorph 3C-SiC (cubic, space group $F\bar{4}3m$). The band gaps are also indirect in this case but noticeably smaller than estimated for 4H-SiC (Fig.5a,b). (Strain-induced band lifting effects are fully taken into consideration in our first-principles DFT results.) For instance, in the absence of strain E_g^{HSE06} amounts to 2.3 eV and at $\eta = -7\%$ to 1.3 eV. The η -induced band-gap variations in 3C-SiC resemble those calculated for 4H-SiC but they are more regular and somewhat larger. Likewise, the vibrational stability of the system is not affected by the

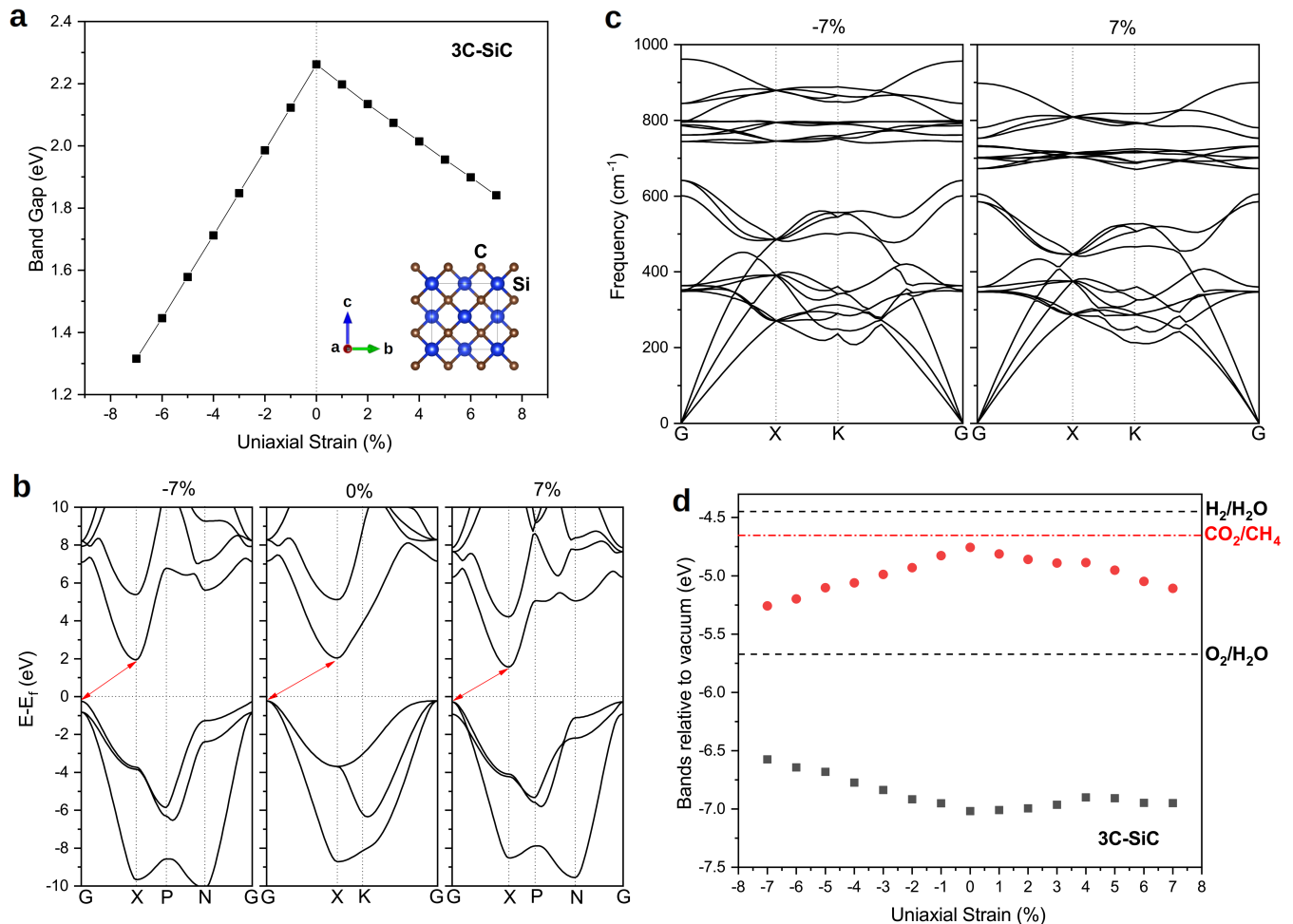


FIG. 5. First-principles analysis of the optoelectronic, vibrational, and band alignment properties of non-piezoelectric 3C-SiC. **a** Band-gap variation induced by uniaxial strain. **b** Dependence of the electronic band structure on uniaxial strain and reciprocal space point. **c** Phonon frequencies estimated as a function of uniaxial strain and reciprocal space point. **d** Effect of uniaxial strain on the band alignments of the crystal as referred to the vacuum level. The VBT and CBB energy levels are represented with solid grey squares and red circles, respectively.

lattice strain (Fig.5c). Nonetheless, the band alignments of non-piezoelectric 3C-SiC under strain behave radically different from those of piezoelectric 4H-SiC (Fig.5d). In particular, the induced VBT and CBB shifts are quite small (i.e., at most ≈ 0.5 eV) and not proportional to the applied strain (i.e., essentially they seem to follow the η -driven E_g^{HSE06} variations found in both compressive and tensile sides). Consequently, the water-splitting photocatalytic properties of non-piezoelectric 3C-SiC cannot be effectively tuned via uniaxial stress and the system remains largely unsuitable for green hydrogen production (i.e., appropriate straddling of the OER and HER energy levels is never achieved through η).

For the sake of completeness and motivated by the fact that previous experimental and computational studies have shown that ZnO is a promising water-splitting photocatalytic material [11, 20–22, 40–42], we explicitly estimated the η -induced band-gap and band-alignment

variations for the wurtzite phase of this material. Figure 6 shows the results of our first-principles calculations carried out for piezoelectric ZnO (hexagonal symmetry, space group $P6_3mc$). Strain-induced band lifting effects are fully taken into consideration in our first-principles DFT results. Under (compressive) tensile uniaxial strain the band gap of wurtzite ZnO remains direct and its size steadily (increases) decreases (Fig.6a-b). The estimated E_g variation is less pronounced than found in SiC (Figs.4-5), although more regular. For example, the band-gap reduction (increase) attained at the highest tensile (compressive) strain considered here is of $\approx 11\%$ ($\approx 6\%$). At the same time, the vibrational stability of wurtzite ZnO is pertinently conserved under uniaxial strain (Fig.6c). The influence of uniaxial strain in the band alignments of ZnO (Fig.6d) is qualitatively very similar to that found in 4H-SiC (Fig.4d). In particular, both the VBT and CBB levels are shifted towards more (less) negative po-

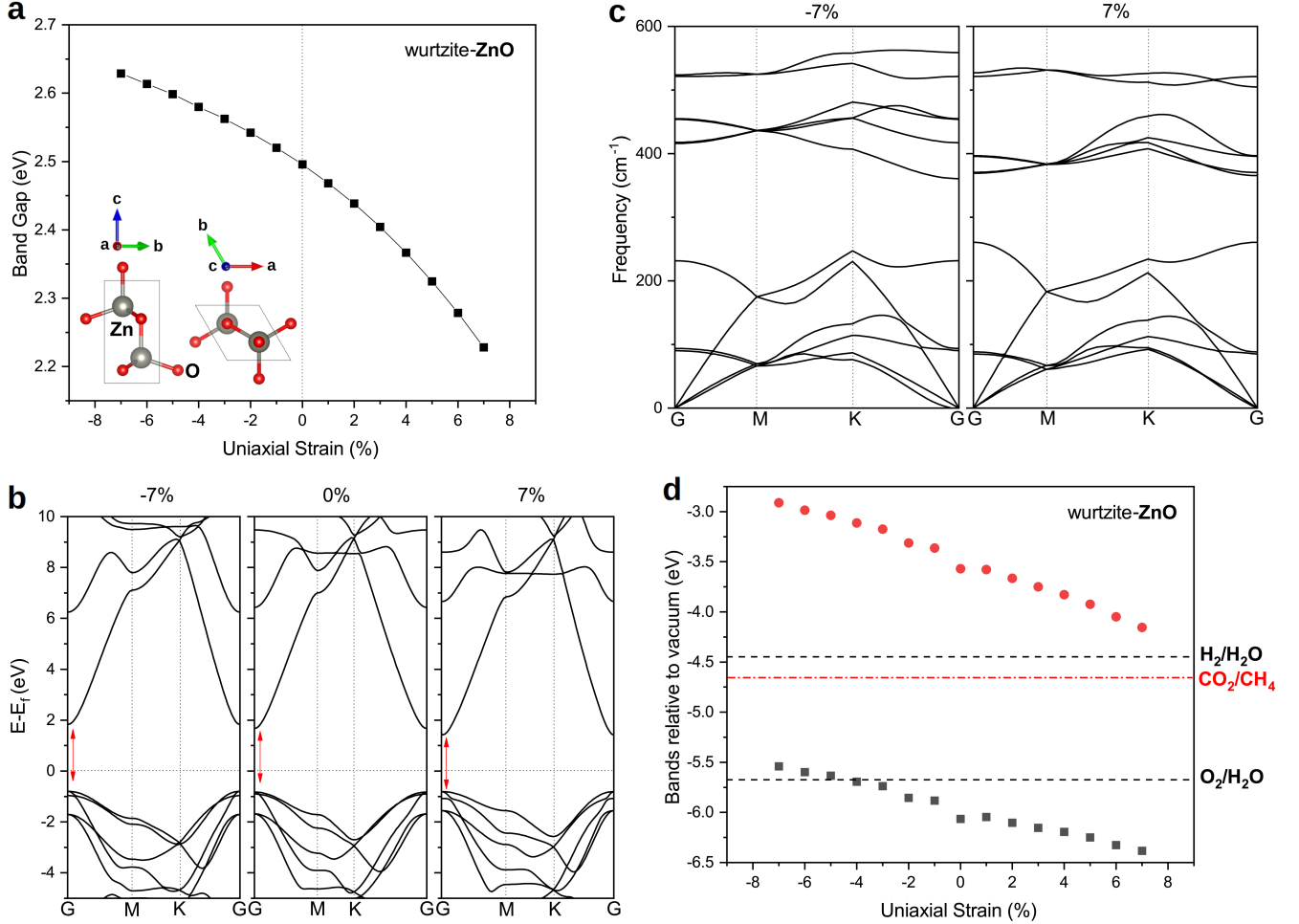


FIG. 6. First-principles analysis of the optoelectronic, vibrational, and band alignment properties of wurtzite ZnO. **a** Band-gap variation induced by uniaxial strain. **b** Dependence of the electronic band structure on uniaxial strain and reciprocal space point. **c** Phonon frequencies estimated as a function of uniaxial strain and reciprocal space point. **d** Effect of uniaxial strain on the band alignments of the crystal as referred to the vacuum level. The VBT and CBB energy levels are represented with solid grey squares and red circles, respectively.

tential values under tensile (compressive) strains and the induced potential variations are quasi linear. The $dV/d\eta$ values estimated for wurtzite ZnO, however, are roughly two times smaller than those found in 4H-SiC. Interestingly, according to our calculations the VBT and CBB positions in unstrained ZnO are already quite optimal for driving the water splitting reaction hence very small structural distortions should be enough to optimally adjust its piezo-photocatalyst performance.

Several general conclusions can be extracted from the results presented in this section. First, the band alignments of piezoelectric materials in fact can be tailored by uniaxial strain in a systematic and efficient manner. Second, the η -induced band-alignment changes predicted by the simple PPC model are physically well-motivated and thus can be used for the screening of potential piezo-photocatalytic materials. (Actually, whenever the band alignments of a piezoelectric compound

are known the simple PPC model can be used to roughly estimate the amount of tensile or compressive uniaxial strain that is necessary to shift them towards optimal levels.) And third, the list of potential water-splitting piezo-photocatalytic materials enclosed in Table II should be regarded as trustworthy, hence it may be key in guiding strain-assisted experiments in the field of green hydrogen production.

DISCUSSION

The two rankings of piezo-photocatalytic materials enclosed in Tables I and II, respectively deduced from the DFT data found in the MP database and our refined DFT calculations, display appreciable quantitative differences. For instance, in Table I the value of the reported piezoelectric potential coefficients are typically smaller than in

Table II and the top positions in the first list are predominantly occupied by oxide perovskites (whereas KIO_3 in the first position of Table II is an inorganic salt). Furthermore, upon refinement of the structural, piezoelectric and dielectric DFT data several materials initially classified as suitable water-splitting piezo-photocatalysts in Table I were finally discarded and not included in Table II (e.g., KNO_3 , GaP and TlF), whereas few materials that initially were discarded finally were included in Table II (i.e., ZnO, CdS and ScCuS_2). On the other hand, at the qualitative level both materials rankings are generally equivalent since oxide, nitride and halide compounds are consistently presented as the most promising. Therefore, for piezo-photocatalyst screening purposes the DFT data contained in the MP database should be regarded as of sufficient quality. For the rest of this section, however, we will concentrate our analysis on the materials reported in Table II.

The first of all ranked piezo-photocatalysts, KIO_3 , appears to be auspicious both in terms of band alignments tunability (i.e., largest $\alpha_{\eta}^{\text{rev}}$ value) and economical costs (i.e., all the integrating elements are abundant); however, this material is soluble in water and therefore is of little practical relevance in the context of water splitting photocatalysis. Similar water solubility and water reactivity drawbacks are posed by the compounds SeBr and PI_3 (Table II), which should neither be contemplated in the context of green hydrogen production applications. Notwithstanding such limitations, these water unsuited piezo-photocatalytic materials could turn out to be useful for catalyzing other green chemistry reactions not requiring of aqueous media (e.g., CO_2 reduction [43]) hence we cautiously keep them in our list of selected candidates.

In the second position of Table II, it appears the perovskite oxide KNbO_3 for which recently its great piezo-photocatalytic potential has been experimentally demonstrated [29, 30]. In fact, according to our DFT calculations KNbO_3 possesses superior photocatalytic band structure features than BaTiO_3 (which appears in the fifth position), namely, a slightly smaller band gap and a larger $\alpha_{\eta}^{\text{rev}}$ coefficient. Likewise, ZnO, another known photocatalytic and piezo-photocatalytic compound, shows up in the ninth position of our definitive list, which comes to assure the reliability of our computational screening method.

In the third and fourth positions of Table II, we find LaN and PtF_4 , two materials that, to the best of our knowledge, have not been investigated thus far as potential water splitting photocatalysts in spite of their appropriate band gap and large band alignments tunability. PtF_4 , however, contains precious elements hence its main drawback may be the high costs associated with its manufacturing. Similar expense limitations may also affect the three chalcogenide compounds BiTeCl, MgTe and BiTeI appearing in the eleventh, thirteenth and fifteenth positions of Table II, respectively, since they contain the rare-earth element Te. Concerning these latter systems, it may be interesting to explore whether similar piezo-

photocatalytic performances can be attained by means of chemical substitutions based on the more abundant chalcogenide species Se and S.

The two chalcogenides CdS and ScCuS_2 show up in the sixth and eighth positions of Table II, respectively. CdS is an already known semiconductor material in the context of photocatalytic hydrogen production since it presents suitable band edge positions and a band gap that is responsive to visible light [3]. Actually, CdS becomes an excellent photocatalyst for H_2 evolution under visible light irradiation when aided by hole scavenger co-catalysts that help to prevent possible photocorrosion issues [44]. Thus, in view of its high ranking position in Table II, right after BaTiO_3 , and already appropriate photocatalytic features in the absence of mechanical stimulation, CdS emerges as a highly promising piezo-photocatalytic compound. ScCuS_2 , on the other hand, is a relatively unknown material that only recently has been investigated in the context of possible thermoelectric and photovoltaic applications by means of first-principles simulation methods [45, 46]. Nevertheless, according to our DFT calculations, this material is highly auspicious for photocatalysis due to its great band alignment tunability under strain and favorable hydrogen evolution activity (see below).

Furthermore, GaN, a well-known direct band-gap semiconductor extensively used in light-emitting applications, appears in the twelfth position of our ranking. The photocatalytic activity of this material in water-splitting hydrogen production has been already assessed and seems to be quite promising [47, 48]. Since GaN is a well-known piezoelectric and technologically relevant material, it is likely that its piezo-photocatalytic performance will be eventually assessed; however, to the best of our knowledge, this possibility has not been yet addressed in the scientific literature. On this regard, our high-throughput computational screening suggests that it could be beneficial to consider also the alike nitride LaN since this compound ranks in the third position of our candidate piezo-photocatalysts list and in terms of production costs seems to be similar to GaN.

By overlooking the water soluble and reacting (i.e., KIO_3 , SeBr and PI_3), high cost (i.e., PtF_4 , BiTeCl, MgTe and BiTeI) and already known (i.e., KNbO_3 , BaTiO_3 and ZnO) piezo-photocatalytic compounds reported in Table II, we are left with six promising candidates: the nitrides LaN and GaN, the chalcogenides CdS and ScCuS_2 , the halide AgI and the semiconductor SiC. Most of these materials (i.e., all except ScCuS_2) are already known from their use in numerous applications ranging from industry and electronics to energy conversion, and they can be efficiently produced in different morphologies and large quantities (e.g., AgI and SiC [49, 50]). Therefore, even if the piezoelectric coefficient of some of them are noticeably smaller than those of, for instance, KNbO_3 and PtF_4 , it is certainly worth assessing their actual water-splitting piezo-photocatalytic qualities in experiments.

The overall photocatalytic performance of a piezoelec-

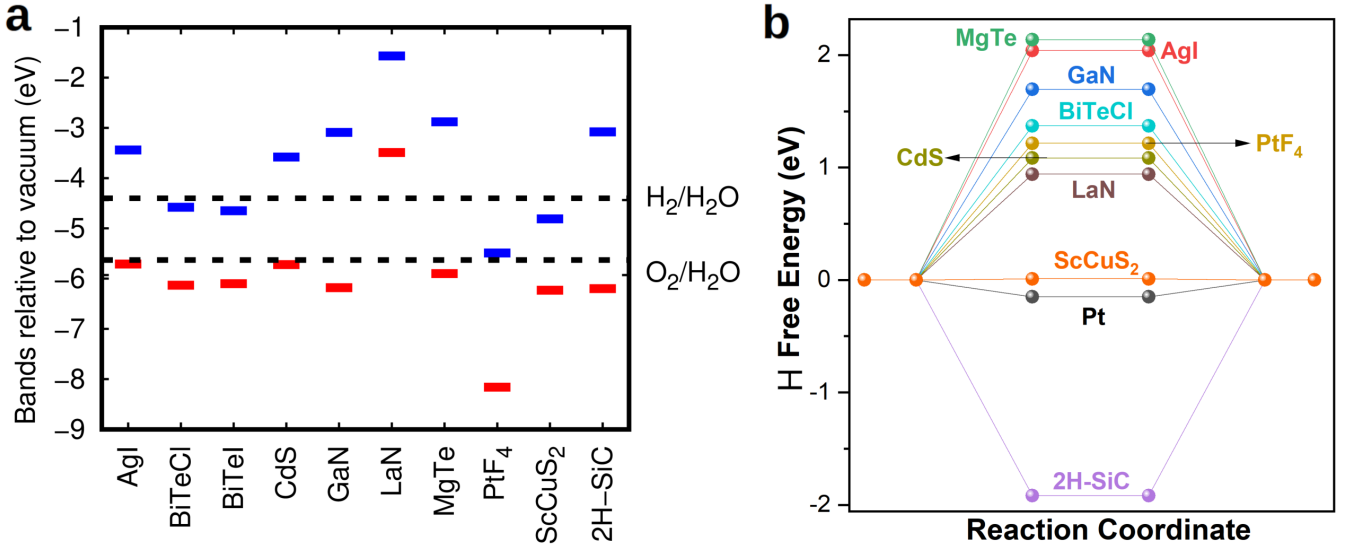


FIG. 7. First-principles estimation of the **a** band alignments and **b** hydrogen adsorption free energy of the most promising piezo-photocatalytic materials coming out from our computational screening in the absence of uniaxial strain.

tric material in fact does not solely depend on its band gap and band alignment tunabilities, which are the two main aspects that have been considered throughout the present work. Other features like the initial band positions in the unstrained state, the recombination rate of photogenerated carriers and surface overpotentials for the hydrogen and oxygen evolution reactions, for instance, may be also determinant. Theoretical evaluation of some of these properties, however, involve cumbersome calculations hence we leave them for future work. Nevertheless, for the sake of completeness and to motivate experimental efforts, we evaluated the zero-strain band alignments and hydrogen evolution energetics of the candidate piezo-photocatalysts listed in Table II, excepting those materials that pose water-related issues (i.e., KIO₃, SeBr and PI₃) and were already known (i.e., KNbO₃, BaTiO₃ and ZnO).

Figure 7a shows the band edge positions of the screened candidate piezo-photocatalysts estimated at zero strain. Except for PtF₄ and LaN, the obtained results appear to be all very encouraging. For instance, compounds AgI, CdS, GaN, MgTe and 2H-SiC satisfactorily straddle the OER and HER potentials whereas BiTeCl, BiTeI and ScCuS₂ practically succeed in doing so. In all these cases, therefore, employing strain strategies to adjust their band edge positions to optimal values appears to be fully justified.

Figure 7b shows the calculated free energy of an hydrogen atom adsorbed on the surface of the candidate piezo-photocatalysts, ΔG_{H} (Methods), a common descriptor employed for the evaluation of HER activity [51, 52]. An ideal HER catalyst, like Pt, should interact very weakly with hydrogen and thus render ΔG_{H} values close to zero. According to our DFT calculations, ScCuS₂ is a superb HER material since the corresponding ΔG_{H} is smaller

than that of Pt and practically null. In order of decreasing HER performance, LaN, CdS, PtF₄, BiTeCl and GaN follow after ScCuS₂. MgTe, AgI and 2H-SiC, on the other hand, seem to interact too strongly with hydrogen other, without further modifications, HER activity may be inhibited on the surface of these materials. Interestingly, we found that in some cases ΔG_{H} can be significantly changed by uniaxial strain (Supplementary Fig.3). Specifically, in PtF₄ and ScCuS₂ the sign of the H adsorption free energy can be reversed by means of modest η 's, thus suggesting the possibility of making ΔG_{H} arbitrarily small by selecting the right strain. In 2H-SiC, we also found that ΔG_{H} can be reduced by roughly 25% of its size via application of a 5% tensile strain.

CONCLUSIONS

We have presented a first-principles high-throughput screening of potential bulk piezo-photocatalytic materials able to accelerate the production of green hydrogen from water under sunlight when exposed to ultrasound waves and/or mechanical actuation. Our computational sieve relies on the DFT information found in the Materials Project database, which comprises about 1,000 bulk piezoelectrics, and an easy-to-compute bulk material descriptor deduced from a simple “piezoelectric plate capacitor” electrostatic model. In short, ideal piezo-photocatalysts should simultaneously exhibit large piezoelectric stress coefficients and small dielectric constants, two qualities that typically oppose each other, besides reasonable band gaps and VBT and CBB energy levels in the unstrained state. Already known good piezo-photocatalysts were retrieved by our computational searches (i.e., KNbO₃, BaTiO₃ and ZnO)

while some other compounds previously overlooked in the context of photocatalysis were also identified as very promising. Specifically, it was found that, in terms of strain-driven band-alignment tunability, the piezo-photocatalytic water splitting ability of the nitrides LaN and GaN, the halides PtF₄ and AgI, the chalcogenides BiTeCl, BiTeI, MgTe, CdS and ScCuS₂ and the semiconductor SiC may be comparable to those of BaTiO₃ and ZnO. Other potential piezo-photocatalysts like bulk KIO₃ and PI₃ were also recognized in spite of their inappropriateness to work in aqueous environments (hence in practice are not suitable for water-splitting photocatalytic applications). The introduced piezo-photocatalyst screening approach is general and can be also applied to other important families of materials not considered in this study (e.g., two-dimensional compounds and solid solutions). Therefore, the present computational work advances knowledge in the field of state-of-the-art photocatalytic materials and is expected to motivate original and prolific experimental investigations in the context of sustainable hydrogen production driven by sunlight.

METHODS

First-principles calculations. First-principles calculations based on density functional theory (DFT) [26–28] were performed to simulate and analyze the influence of uniaxial strain, η , on the optoelectronic, vibrational and band alignment properties of piezo-photocatalytic materials. The PBEsol functional [33] was used as it is implemented in the VASP software package [26]. We employed the “projector augmented wave” method to represent the ionic cores [53] by considering the most relevant electrons of each atomic species as valence. Wave functions were represented in a plane-wave basis truncated at 800 eV. For integrations within the Brillouin zone (BZ) of all materials we employed Monkhorst-Pack \mathbf{k} -point grids [54] of spacing $2\pi \times 0.01 \text{ \AA}^{-1}$. Uniaxially strained bulk geometry relaxations were performed with a conjugate-gradient algorithm that allowed for volume variations while imposing the structural constraints defining uniaxial strain [12]. In our simulations, uniaxial strain is defined as $\eta = (c - c_0)/c_0$, where c_0 represents the length of the strained lattice vector in the absence of any stress. Positive η values are considered tensile uniaxial strains and $\eta < 0$ compressive. Periodic boundary conditions were applied along the three directions defined by the lattice vectors hence possible surface effects were completely neglected in the bulk simulations (not so in the slab simulations, see below). The relaxations were halted when the forces acting on the atoms were all below $0.005 \text{ eV} \cdot \text{\AA}^{-1}$. By using these technical parameters we obtained zero-temperature energies that were converged to within 0.5 meV per formula unit. Uniaxial strain conditions were simulated at $\Delta\eta = 1\%$ intervals. In order to estimate accurate dielectric, piezoelectric and band gap properties, we employed the range-separated hybrid

HSE06 exchange-correlation functional [34] to perform single-point calculations on the equilibrium geometries determined at the PBEsol level [55].

To estimate phonon frequencies we employed the “small-displacement” approach [56], in which the force-constant matrix of the crystal is calculated in real space by considering the proportionality between the atomic displacements and forces when the former are sufficiently small (in the present study this condition was satisfied for atomic displacements of 0.02 \AA). Large supercells containing hundreds of atoms were employed to guarantee that the elements of the force-constant matrix presented practically negligible values at the largest atomic separations. The computation of the nonlocal parts of the pseudopotential contributions were performed in reciprocal space in order to maximise the numerical accuracy of the computed forces. Once a force-constant matrix was determined, we Fourier transformed it to obtain the phonon frequencies for any arbitrary \mathbf{k} -point in the first BZ. This latter step was performed with the PHONOPY code [57], in which the translational invariance of the system was exploited to ensure that the three acoustic branches were exactly zero at the Γ point. Central differences for the atomic forces, that is, both positive and negative atomic displacements, were considered.

To calculate accurate band alignments we followed the work done by Moses and co-workers on binary semiconductors [58]. Briefly, both bulk and slab calculations were performed from which the alignment of the electrostatic potential within the semiconductor material could be obtained relative to the vacuum level. From the slab calculations, the difference between the average electrostatic potential within the semiconductor material and in vacuum was obtained. From the bulk calculations, the band structure shifts relative to the average electrostatic potential were determined. These calculations were performed at each η point and involved the estimation of macroscopic and planar average potentials. The planar potential was computed by averaging potential values within a well defined plane (for instance, perpendicular to the surface of the slab), and the macroscopic potential was obtained by taking averages of the planar potential over distances of one unit cell along the chosen direction [59, 60]. The slab systems were thick enough to ensure that the electron density in the center of the slab was practically equal to that in the bulk material. We found that $\approx 2.0 \text{ nm}$ thick semiconductor slabs (e.g., around 8 SiC layers) accompanied by similarly large portions of vacuum provided sufficiently well converged results for the electrostatic potential and surface energy (Supplementary Fig.4). Band alignments were systematically estimated at the geometrical center of the slabs. A standard hydrogen passivation scheme [61] was employed in the geometry relaxations of the wurtzite ZnO slabs in order to appropriately determine the relevant macroscopic and planar average potential levels (Supplementary Fig.5).

High-throughput screening. The high-throughput screening of potential piezo-photocatalyst was performed using the Matminer package [62]. A pre-existing dataset containing about 1,000 piezoelectric materials was loaded from the Materials Project database [23]. Based on our PPC model, the parameters needed for the high-throughput screening were the thickness (c), dielectric constant (ϵ) and piezoelectric constant (e_{33}) of each considered compound (Results section). The piezoelectric constants of such materials were retrieved from the piezoelectric tensors provided in the same dataset, and their thicknesses were approximated by the mean average of the three corresponding lattice parameters. The value of the dielectric constants and energy band gaps (E_g) were acquired from the Materials Project (MP) database via the corresponding materials mp-ID's; compounds for which the dielectric properties were not reported in the MP database were dropped from our high-throughput screening. Therefore, it is possible that few piezoelectric materials with potentially high piezo-photocatalytic tunability were overlooked in our analysis.

Hydrogen evolution reaction (HER) performance. In addition to the band gap and band alignments, we also evaluated the energetics of the hydrogen evolution reaction (HER) for the screened photocatalytic materials. To do this, we calculated the adsorption free energy of one hydrogen atom (ΔG_H) on the materials

surface, which was obtained through the equation:

$$\Delta G_H = \Delta E_H + \Delta E_{ZPE} - T\Delta S, \quad (6)$$

where ΔE_H is the hydrogen atom adsorption energy and ΔE_{ZPE} and ΔS the zero-point energy and entropy differences between the hydrogen atom adsorbed on the materials surface and in gas phase, respectively. The contribution from the catalysts to both ΔE_{ZPE} and ΔS are very small and thus are neglected. The ΔE_{ZPE} term was calculated like the difference between the zero point energy of the adsorbed hydrogen atom and one half of the zero point energy of a H_2 gas molecule, namely:

$$\Delta E_{ZPE} = E_{ZPE}^H - \frac{1}{2}E_{ZPE}^{H_2}. \quad (7)$$

The size of the ΔE_{ZPE} term is usually small and of the order of ~ 0.01 eV [63]. Meanwhile, ΔS was taken equal to minus one half of the experimental entropy of a H_2 gas molecule under standard thermodynamic conditions (i.e., 298 K and 1 atm), which leads to $T\Delta S = -0.2$ eV [64].

DATA AVAILABILITY

The data that support the findings of this study are available from authors Z.L. and C.C. upon reasonable request.

-
- [1] International Energy Agency (2019). The future of hydrogen, IEA. Paris <https://www.iea.org/reports/the-future-of-hydrogen>
- [2] Idriss, H. Hydrogen production from water: past and present. *Curr. Opin. Chem. Eng.* **29**, 74 (2020).
- [3] Kudo, A. & Miseki, Y. Heterogeneous photocatalyst materials for water splitting. *Chem. Soc. Rev.* **38**, 253 (2009).
- [4] Chen, S., Takata, T. & Domen, K. Particulate photocatalysts for overall water splitting. *Nat. Rev. Mater.* **2**, 17050 (2017).
- [5] Asahi, R., Morikawa, T., Ohwaki, T., Aoki, K. & Taga, Y. Visible-light photocatalysis in nitrogen-doped titanium oxides. *Science* **293**, 269 (2001).
- [6] Mofarah, S. S., *et al.*, Coordination polymer to atomically thin, holey, metal-oxide nanosheets for tuning band alignment. *Adv. Mater.* **31**, 1905288 (2019).
- [7] Bahmanrokh, G., Cazorla, C., Mofarah, S. S., Shahmiri, R., Yao, Y., Ismail, I., Chen, W.-F., Koshy, P. & Sorrell, C. C. Band gap engineering of Ce-doped anatase TiO_2 through solid solubility mechanisms and new defect equilibria formalism. *Nanoscale* **12**, 4916 (2020).
- [8] Xu, Y., Mofarah, S. S., Mehmood, R., Cazorla, C., Koshy, P. & Sorrell, C. C. Design strategies for ceria nanomaterials: untangling key mechanistic concepts. *Mater. Horiz.* **8**, 102 (2021).
- [9] Park, H., Kim, H.-I., Moon, G.-H. & Wonyong, C. Photoinduced charge transfer processes in solar photocatalysis based on modified TiO_2 . *Energy Environ. Sci.* **9**, 411 (2016).
- [10] Takanabe, K. Photocatalytic water splitting: Quantitative approaches toward photocatalyst by design. *ACS Catal.* **7**, 8006 (2017).
- [11] Liu, Z., Menéndez, C., Shenoy, J., Hart, J. N., Sorrell, C. C. & Cazorla, C. Strain engineering of oxide thin films for photocatalytic applications. *Nano Energy* **72**, 104732 (2020).
- [12] Liu, Z., Wang, B & Cazorla, C. Mechanical and electronic properties of CeO_2 under uniaxial tensile loading: A DFT study. *Materialia* **15**, 101050 (2021).
- [13] Zhang, L., Chen, J., Fan, L., Diéguez, O., Cao, J., Pan, Z., Wang, Y., Wang, J., Kim, M., Deng, S., Wang, J., Wang, H., Deng, J., Yu, R., Scott, J. F. & Xing, X. Giant polarization in super-tetragonal thin films through interphase strain. *Science* **361**, 494 (2019).
- [14] Hu, S., Wang, Y., Cazorla, C. & Seidel, J. Strain-enhanced oxygen dynamics and redox reversibility in topotactic $SrCoO_{3-\delta}$ ($0 \leq \delta \leq 0.5$). *Chem. Mater.* **29**, 708 (2017).
- [15] Dang, C., Chou, J.-P., Dai, B., Chou, C.-T., Yang, Y., Fan, R., Lin, W., Meng, F., Hu, A., Zhu, J., Han, J., Minor, A. M., Li, J. & Lu, Y. Achieving large uniform ten-

- sile elasticity in microfabricated diamond. *Science* **371**, 76 (2021).
- [16] Phan, H.-P., Nguyen, T.-K., Dinh, T., Ina, G., Kermany, A. R., Qamar, A., Han, J., Namazu, T., Maeda, R., Dao, D. V. & Nguyen, N.-T. Ultra-high strain in epitaxial silicon carbide nanostructures utilizing residual stress amplification. *Appl. Phys. Lett.* **110**, 141906 (2017).
- [17] Blagov, A. E., Kovalchuk, M. V., Pisarevskii, Y. V. & Prosekov, P. A. Control of the crystal lattice strain gradient caused by low-frequency ultrasound. *Crystallogr. Rep.* **53**, 379 (2008).
- [18] Truell, R., Elbaum, C. & Chick, B. B. Ultrasonic methods in solid state physics. New York, Academic Press (1969).
- [19] Wu, W. & Wang, Z. Piezotronics and piezo-phototronics for adaptive electronics and optoelectronics. *Nat. Rev. Mater.* **1**, 16031 (2016).
- [20] Tu, S., Guo, Y., Zhang, Y., Hu, C., Zhang, T., Ma, T. & Huang, H. Piezocatalysis and piezo-photocatalysis: Catalysts classification and modification strategy, reaction mechanism, and practical application. *Adv. Funct. Mater.* **30**, 2005158 (2020).
- [21] Liang, Z., Yan, C.-F., Rtimi, S. & Bandara, J. Piezoelectric materials for catalytic/photocatalytic removal of pollutants: Recent advances and outlook. *Appl. Catal. B: Environ.* **241**, 256 (2019).
- [22] Sakthivel, T., Venugopal, G., Durairaj, A., Vasanthkumar, S. & Huang, X. Utilization of the internal electric field in semiconductor photocatalysis: A short review. *J. Ind. Eng. Chem.* **72**, 18 (2019).
- [23] de Jong, M., Chen, W., Geerlings, H., Asta, M. & Persson, K. A. A database to enable discovery and design of piezoelectric materials. *Sci. Data* **2**, 150053 (2015).
- [24] Dash, S., Pradhan, D. K., Kumari, S., Rahaman, R. M., Cazorla, C., Brajesh, K., Kumar, A., Thomas, R., Rack, P. D. & Pradhan, D. K. Enhanced ferroelectric and piezoelectric properties of BCT-BZT at the morphotropic phase boundary driven by the coexistence of phases with different symmetries. *Phys. Rev. B* **104**, 224105 (2021).
- [25] Cazorla, C. & Stengel, M. Electrostatic engineering of strained ferroelectric perovskites from first principles. *Phys. Rev. B* **92**, 214108 (2015).
- [26] Kresse, G. & Fürthmüller, J. Efficient iterative schemes for ab initio total-energy calculations using a plane-wave basis set. *Phys. Rev. B* **54**, 11169 (1996).
- [27] Cazorla, C. The role of density functional theory methods in the prediction of nanostructured gas-adsorbent materials. *Coord. Chem. Rev.* **300**, 142 (2015).
- [28] Cazorla, C. & Boronat, B. Simulation and understanding of atomic and molecular quantum crystals. *Rev. Mod. Phys.* **89**, 035003 (2017).
- [29] Yu, D., Liu, Z., Zhang, J., Li, S., Zhao, Z., Zhu, L., Liu, W., Lin, Y., Liu, H. & Zhang, Z. Enhanced catalytic performance by multi-field coupling in KNbO₃ nanostructures: Piezo-photocatalytic and ferro-photoelectrochemical effects. *Nano Energy* **58**, 695 (2019).
- [30] Zhang, Y., Shen, G., Sheng, C., Zhang, F. & Fan, W. The effect of piezo-photocatalysis on enhancing the charge carrier separation in BaTiO₃/KNbO₃ heterostructure photocatalyst. *Appl. Surf. Sci.* **562**, 150164 (2021).
- [31] Moustakas, T. D. & Paiella, R. Optoelectronic device physics and technology of nitride semiconductors from the UV to the terahertz. *Rep. Prog. Phys.* **80**, 106501 (2017).
- [32] J. P. Perdew. Density functional theory and the band gap problem. *Int. J. Quantum Chem.* **19**, 497 (1986).
- [33] Perdew, J. P., Ruzsinszky, A., Csonka, G. I., Vydrov, O. A., Scuseria, G. E., Constantin, L. A., Zhou, X. & Burke, K. Restoring the density-gradient expansion for exchange in solids and surfaces. *Phys. Rev. Lett.* **100**, 136406 (2008).
- [34] Krukau, A. V., Vydrov, O. A., Izmaylov, A. F. & Scuseria, G. E. Influence of the exchange screening parameter on the performance of screened hybrid functionals. *J. Chem. Phys.* **125**, 224106 (2006).
- [35] Park, J.-S. Comparison study of exchange-correlation functionals on prediction of ground states and structural properties. *Curr. Appl. Phys.* **22**, 61 (2021).
- [36] Liu, H., She, G., Mu, L. & Xi, W. Porous SiC nanowire arrays as stable photocatalyst for water splitting under UV irradiation. *Mater. Res. Bull.* **47**, 917 (2012).
- [37] Yasuda, T., Kato, M., Ichimura, M. & Hatayama, T. SiC photoelectrodes for a self-driven water-splitting cell. *Appl. Phys. Lett.* **101**, 053902 (2012).
- [38] Wang, D., Guo, Z., Peng, Y. & Yuan, W. Visible light induced photocatalytic overall water splitting over micro-SiC driven by the Z-scheme system. *Catalysis Commun.* **61**, 53 (2015).
- [39] Wang, D., Guo, Z., Peng, Y. & Yuan, W. A simple route to significant enhancement of photocatalytic water oxidation on BiVO₄ by heterojunction with SiC. *Chem. Eng. J.* **281**, 102 (2015).
- [40] Hamid, S. B. A., Teh, S. J. & Lai, C. W. Photocatalytic Water Oxidation on ZnO: A Review. *Catalysts* **7**, 93 (2017).
- [41] Zhang, X., Zhou, Y.-Z., Wu, D.-Y., Liu, X.-H., Zhang, R., Liu, H., Dong, C.-K., Yang, J., Kulinich, S. A. & Du, X.-W. ZnO nanosheets with atomically thin ZnS overlayers for photocatalytic water splitting. *J. Mater. Chem. A* **6**, 9057 (2018).
- [42] Cao, C., Zhang, B. & Lin, S. p-type ZnO for photocatalytic water splitting. *APL Mater.* **10**, 030901 (2022).
- [43] Jiang, C., Nichols, A. W., Walzer, J. F. & Machan, C. W. Electrochemical CO₂ reduction in a continuous non-aqueous flow cell with [Ni(cyclam)]²⁺. *Inorg. Chem.* **59**, 1883 (2020).
- [44] Nasir, J. A., Rehman, Z., Shah, S. N. A., Khan, A., Butler, I. S. & Catlow, C. R. A. Recent developments and perspectives in CdS-based photocatalysts for water splitting. *J. Mater. Chem. A* **8**, 20752 (2020).
- [45] Rugut, E., Joubert, D. & Jones, G. First-principle studies on lattice thermal conductivity and thermoelectric properties of ScCu(S,Se,Te)₂. *Mater. Today Commun.* **26**, 101905 (2021).
- [46] Scanlon, D. O. & Watson, G. W. Stability, geometry, and electronic structure of an alternative I-III-VI₂ material, CuScS₂: A hybrid density functional theory analysis. *Appl. Phys. Lett.* **97**, 131904 (2010).
- [47] Kida, T., Minami, Y., Guan, G., Nagano, N., Akiyama, M. & Yoshida, A. Photocatalytic activity of gallium nitride for producing hydrogen from water under light irradiation. *J. Mater. Sci.* **41**, 3527 (2006).
- [48] Shimosako, N. & Sakama, H. Quantum efficiency of photocatalytic activity by GaN films. *AIP Adv.* **11**, 025019 (2021).
- [49] She, X., Huang, A. Q., Lucía, O. & Ozpineci, B. Review of silicon carbide power devices and their applications.

- IEEE Trans. Indust. Electr.* **64**, 8193 (2017).
- [50] Aznar, A., Lloveras, P., Romanini, M., Barrio, M., Tamarit, J.-L., Cazorla, C., Errandonea, D., Mathur, N. D., Planes, A., Moya, X. & Mañosa, Ll. Giant barocaloric effects over a wide temperature range in superionic conductor AgI. *Nat. Commun.* **8**, 1851 (2017).
- [51] Gao, G. & Du, A. Understanding the activity and selectivity of single atom catalysts for hydrogen and oxygen evolution via ab initial study. *Catal. Sci. Technol.* **8**, 996 (2018).
- [52] Uosaki, K., Elumalai, G., Dinh, H. C., Lyalin, A., Taketsugu, T. & Noguchi, H. Highly efficient electrochemical hydrogen evolution reaction at insulating boron nitride nanosheet on inert gold substrate. *Sci. Rep.* **6**, 32217 (2016).
- [53] Blöchl P. E. Projector augmented-wave method. *Phys. Rev. B* **50**, 17953 (1994).
- [54] Monkhorst, H. J. & Pack, J. D. Special points for Brillouin-zone integrations. *Phys. Rev. B* **13**, 5188 (1976).
- [55] Shenoy, J., Hart, J. N., Grau-Crespo, R., Allan, N. L. & Cazorla, C. Mixing thermodynamics and photocatalytic properties of GaP-ZnS solid solutions. *Adv. Theory Simul.* **2**, 1800146 (2019).
- [56] Alfè, D. PHON: A program to calculate phonons using the small displacement method. *Comp. Phys. Commun.* **180**, 2622 (2009).
- [57] Togo, A. & Tanaka, I. First principles phonon calculations in materials science. *Scr. Mater.* **108**, 1 (2015).
- [58] Moses, P. G., Miao, M., Yan, Q., & Van de Walle, C. G. Hybrid functional investigations of band gaps and band alignments for AlN, GaN, InN, and InGaN. *J. Chem. Phys.* **134**, 084703 (2011).
- [59] Baldereschi, A., Baroni, S. & Resta, R. Band offsets in lattice-matched heterojunctions: A model and first-principles calculations for GaAs/AlAs. *Phys. Rev. Lett.* **61**, 734 (1988).
- [60] Cazorla, C. & Stengel, M. First-principles modeling of Pt/LaAlO₃/SrTiO₃ capacitors under an external bias potential. *Phys. Rev. B* **85**, 075426 (2012).
- [61] Shiraishi, K. A new slab model approach for electronic structure calculation of polar semiconductor surface. *J. Phys. Soc. Jpn.* **59**, 3455 (1990).
- [62] Ward, L., *et al.* Matminer: An open source toolkit for materials data mining. *Comput. Mater. Sci.* **152**, 60 (2018).
- [63] Norskov, J. K., Bligaard, T., Logadottir, A., Kitchin, J., Chen, J. G., Pandelov, S. & Stimming, U. Trends in the exchange current for hydrogen evolution. *J. Electrochem. Soc.* **152**, J23-J26 (2005).

- [64] Atkins, P. and de Paula, J. (2014). *Atkins' Physical Chemistry*. 10th Edition, Oxford University Press, Oxford.

ACKNOWLEDGEMENTS

C.C. acknowledges support from the Spanish Ministry of Science, Innovation and Universities under the “Ramón y Cajal” fellowship RYC2018-024947-I. Z.L and B.W. acknowledge support from the National Natural Science Foundation of China (12002402, 11832019), the NSFC original exploration project (12150001), the Project of Nuclear Power Technology Innovation Center of Science Technology and Industry for National Defense (HDLCXZX-2021-HD-035), and the Guangdong International Science and Technology Cooperation Program (2020A0505020005). D.C. acknowledges support from the Australian Research Council Projects (DP210100879, LP190100829).

AUTHOR CONTRIBUTIONS

Z.L. and C.C. conceived the study and planned the research. C.C. proposed the electrostatic modelling of piezo-photocatalyst materials. Z.L. performed the high-throughput computational screening of piezo-photocatalysts based on the Materials Project database. Z.L. and C.C. performed the supplementary and validation first-principles calculations and analysed the results along with the rest of co-authors. The manuscript was written by C.C. with substantial input from the rest of co-authors.

ADDITIONAL INFORMATION

Supplementary information is available in the online version of the paper.

COMPETING FINANCIAL INTERESTS

The authors declare no competing financial interests.